

Temperature-modulated synchronization transition in coupled neuronal oscillators

Yasuomi D. Sato,^{1,2,3,*} Keiji Okumura,⁴ Akihisa Ichiki,⁴ Masatoshi Shiino,⁴ and Hideyuki Câteau^{3,1,†}

¹*Department of Brain Science and Engineering, Graduate School of Life Science and Systems Engineering, Kyushu Institute of Technology, 2-4 Hibikino, Wakamatsu, Kitakyushu 808-0196, Japan*

²*Frankfurt Institute for Advanced Studies (FIAS), Johann Wolfgang Goethe University, Ruth-Moufang-Strasse 1, D-60438 Frankfurt am Main, Germany*

³*RIKEN BSI-TOYOTA Collaboration Center, RIKEN Brain Science Institute, 2-1 Hirosawa, Wako, Saitama 351-0198, Japan*

⁴*Department of Physics, Faculty of Science, Tokyo Institute of Technology, 2-12-1 Ohokayama, Meguro-ku, Tokyo 152-8551, Japan*

(Received 18 November 2011; published 15 March 2012)

We study two firing properties to characterize the activities of a neuron: frequency-current (f - I) curves and phase response curves (PRCs), with variation in the intrinsic temperature scaling parameter (μ) controlling the opening and closing of ionic channels. We show a peak of the firing frequency for small μ in a class I neuron with the I value immediately after the saddle-node bifurcation, which is entirely different from previous experimental reports as well as model studies. The PRC takes a type II form on a logarithmic f - I curve when μ is small. Then, we analyze the synchronization phenomena in a two-neuron network using the phase-reduction method. We find common μ -dependent transition and bifurcation of synchronizations, regardless of the values of I . Such results give us helpful insight into synchronizations tuned with a sinusoidal-wave temperature modulation on neurons.

DOI: [10.1103/PhysRevE.85.031910](https://doi.org/10.1103/PhysRevE.85.031910)

PACS number(s): 87.19.1l, 05.45.Xt, 02.60.Cb, 87.10.Ed

I. INTRODUCTION

Temperature is one of the most significant physical variables in neuronal dynamics. In particular, neuronal activities as representatives of oscillatory or nonlinear dynamics are very sensitive to the temperature through ionic channel gating kinetics [1,2]. The variation in temperature also has a crucial impact on the maximum ionic channel conductance [3,4]. The Hodgkin-Huxley (HH) type model [5] describes the temporal evolution of the membrane potential, where time courses of the ion-channel activations were scaled with the commonly used equation $\mu = Q_{10}^{(T-T_0)/10}$, with temperature T ($^{\circ}\text{C}$), $Q_{10}(\approx 3)$, and $T_0(=6.3^{\circ}\text{C})$ [6]. To obtain the membrane potential dynamics with respect to temperature, T , all activations and inactivations of the channel need to be scaled by μ . Kuang *et al.* [7] have investigated the thermal influence on spiking properties by numerically calculating the thermal dependence of the spiking threshold in the HH model.

However, little is known about temperature dependence of spike synchrony in the nervous system. Prior and Grega experimentally demonstrated increased synchrony between two bursting neurons at low temperatures [8]. Wang and Buzsaki [9] have simulated a partial loss in synchrony with a change of the temperature-scaling-factor value for a network of globally all-to-all coupled identical neurons. They showed that the neurons were dynamically broken into two clusters; the neurons fired synchronously within each cluster and the spike timings of the two clusters alternated in time. They did not discuss how such partial desynchronization occurred with a decrease in temperature. Therefore, it would be very interesting to study temperature-dependent synchronization of neurons.

For this purpose, we need to develop a so-called phase response curve (PRC) for the neuron in question. The PRC

describes the transient change in the cycle period induced by a small stimulus as a function of the phase at which it has been received [10–13]. In general, the PRC can be classified into two types. A type I PRC has almost all positive values (which means the phase advances) while a type II PRC has negative values, meaning phase delays as well. These values are dependent on the phase at which a stimulus is applied. Two excitatory neurons with a type I PRC become synchronized more smoothly than the type II neurons [14]. Thus far, no one has demonstrated the effects of temperature on the PRC and its related synchronous behavior in mutual excitation or inhibition.

Also, we may have to study a frequency-current (f - I) curve for measuring neuronal activity character [15–17]. The curve can be classified into two classes: Class I shows that when I is slowly increased, the neuronal voltage dynamics changes from stationary to oscillatory with zero frequency. Meanwhile, class II means that the onset occurs with nonzero frequency. To find mechanisms for such repetitive firing generation, the stabilities of dynamical states as well as the bifurcation structures in the neuron model were analyzed well [18–20], but the frequency-temperature relation is still unclear.

In experiments [21–23] and model studies [24], only a monotonic frequency increment was observed with increasing temperature. It is thus important to not only study the frequency-temperature-relation-dependent spiking model types but also to investigate how such frequency-temperature relations affect synchronization transition.

We focus on the temperature μ in the ionic channel mechanisms in a neuron, in order to study its effects on the membrane potential dynamics, as well as synchronicity in the two neurons that interact with excitatory chemical synapses, in terms of the current and the synaptic time constant. The two-neuron system is based on the Morris-Lecar (ML) model [25,26]. The ML type, taking a well-known type I PRC, has a common structure with two-dimensional excitability models such as the (V, n)-reduced HH equations [27]. It is modeled by two voltage-sensitive conductances of calcium and potassium.

*sato-y@brain.kyutech.ac.jp; sato@fias.uni-frankfurt.de

†cateau@brain.riken.jp

The chemical synapses employed here are modeled by an α function [28,29].

We investigate the μ dependencies of f itself as well as the f - I curve by analyzing trajectories of the ML model dynamics. We show how firing frequency variations can be related to the shape of the PRC derived together with phase equations by the phase-reduction method [30–32]. By using the phase equation, stabilities of synchronized solutions of the paired system are analyzed in terms of I , μ , and the time constant of excitatory synapses. We find noteworthy bifurcation and transition phenomena of synchronizations. Results of temperature-modulated synchronization transition allow us to explain mechanisms of synchronization-desynchronization transition modulated with sinusoidal-wave temperature. We will give a brief discussion and a conclusion.

II. SPIKING PROPERTIES OF A NEURON MODEL

In this study, we investigate thermal effects on neuronal firing properties of the ML model defined as

$$C_m \frac{dV}{dt} = -g_L(V - V_L) - g_K W(V - V_K) - g_{Ca} m_\infty(V)(V - V_{Ca}) + I, \quad (1)$$

$$\frac{dW}{dt} = \frac{\mu}{\tau_w(V)} (w_\infty(V) - W), \quad (2)$$

with

$$\begin{aligned} m_\infty(V) &= \{1 + \tanh[(V - V_1)/V_2]\}/2, \\ w_\infty(V) &= \{1 + \tanh[(V - V_3)/V_4]\}/2, \\ \tau_w(V) &= 1/\{15.0 \cosh[(V - V_3)/(2V_4)]\}, \end{aligned}$$

where V (mV) and W represent the membrane potential and the gating variable of the K^+ channel, respectively. V_{Ca} , V_K , and V_L represent equilibrium potentials of Ca^{2+} , K^+ , and leak currents, respectively. g_{Ca} , g_K , and g_L are the maximum conductances of corresponding ionic currents. Values of these parameters are set as $C_m = 20 \mu\text{F}/\text{cm}^2$, $V_K = -80$ mV, $V_L = -60$ mV, $V_{Ca} = 120$ mV, $g_L = 2 \mu\text{S}/\text{cm}^2$, $g_K = 8 \mu\text{S}/\text{cm}^2$, $g_{Ca} = 4.0 \mu\text{S}/\text{cm}^2$, $V_1 = -1.2$ mV, $V_2 = 18$ mV, $V_3 = 12$ mV, and $V_4 = 17.4$ mV (see [33]). This parameter setting establishes a nonlinear dynamical structure that saddle-node bifurcation occurs by an upward shift of the cubic V -nullcline with an increase of the current I . We see that increasing I past the critical value $I_{sn} = 39.6935$ results in annihilation of the saddle and node equilibria. The channel kinetics is known to depend on temperature through $\mu = Q_{10}^{(T-T_0)/10}$ appearing in Eq. (2) [6,34].

The kinetics of the synaptic channels is also assumed to have the same μ dependence, because there exist both ionic and receptor channels at the same place on the neuron. The synaptic kinetics is described as

$$\frac{ds}{dt} = \frac{\mu}{\tau_{syn}} (-s + h), \quad (3)$$

$$\frac{dh}{dt} = \frac{\mu}{\tau_{syn}} [-h + \Theta(V)], \quad (4)$$

where the synaptic variable s is driven by the variable h , which is in turn driven by V using a step function Θ with

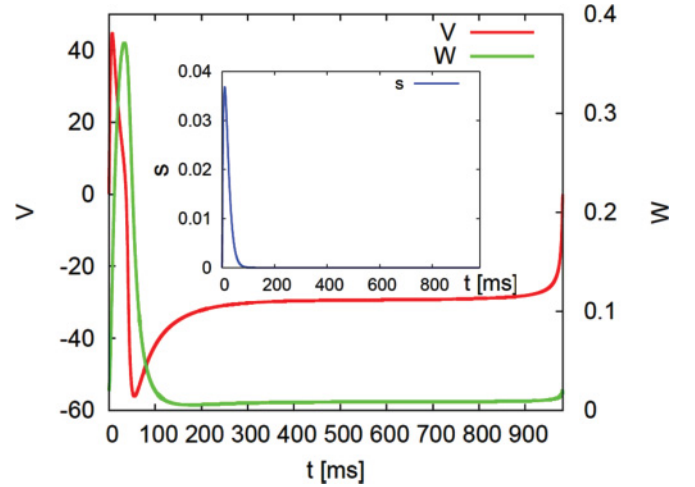


FIG. 1. (Color online) Dynamics of the Morris-Lecar-type spiking model and synaptic potential for V , W , and s . Here we used the parameter set of $\mu = 0.25$, $I = 39.695 \mu\text{A}/\text{cm}^2$, and $\tau_{syn} = 2.5$ ms.

threshold $V_{th} = 0.0$ mV. τ_{syn} (ms) is a synaptic time constant. The dynamics for variables V , W , and s are shown in Fig. 1.

A. Temperature dependence of the membrane dynamics

Let us investigate how the temperature affects the membrane potential dynamics of the ML model at $I = 39.7$, by analyzing the dynamics over the range $0 < \mu \leq 1$. The dynamical trajectories in the W - V plane for $\mu = 1.0, 0.5, 0.15$, and 0.05 [Fig. 2(a)] illustrate that, with small μ values, an upstroke of V is faster and the depolarization is prolonged like a plateau compared to the case with a large μ value, which is found also with the corresponding voltage trajectories as shown in Fig. 2(b). This is simply because smaller values of μ make the potassium channels open more slowly, making for easier depolarization. In either Figs. 2(a) or 2(b), the speed of the dynamics is not explicitly represented. The former only shows a pathway of the movement of (V, W) . Time information is lost in the latter panel since the period of the oscillation is normalized to be unity. As shown in Fig. 2(b), the action potential duration is gradually extended with decreasing values of μ . The simulation may be in agreement with various experimental results for temperature-affected action potential duration [23,35,36].

Figures 2(a) and 2(b) enable us to find that membrane potential dynamics immediately before depolarization for larger μ is extraordinary slow, compared to when μ is small (at least $\mu \leq 0.2$). This is because the trajectory gets closer to the neighborhood of the saddle-node equilibrium, thereby leading to a significant phase delay. However, when μ gradually becomes smaller, the trajectory becomes further from the saddle-node bifurcation location to increase dV/dt [Fig. 2(c)]. Indeed, when μ decreases from 1 to 0.1, dV/dt increases together with the main term in Eq. (1), $-I_{Ca} [-g_{Ca} m_\infty(V)(V - V_{Ca})]$, because $dV/dt \gg dW/dt$ and $-I_{Ca} \gg -I_K$ around $W = 0.007$ [Fig. 2(d)]. Since a firing frequency is approximated as a function of dV/dt , it can be expected that the frequency increases as well.

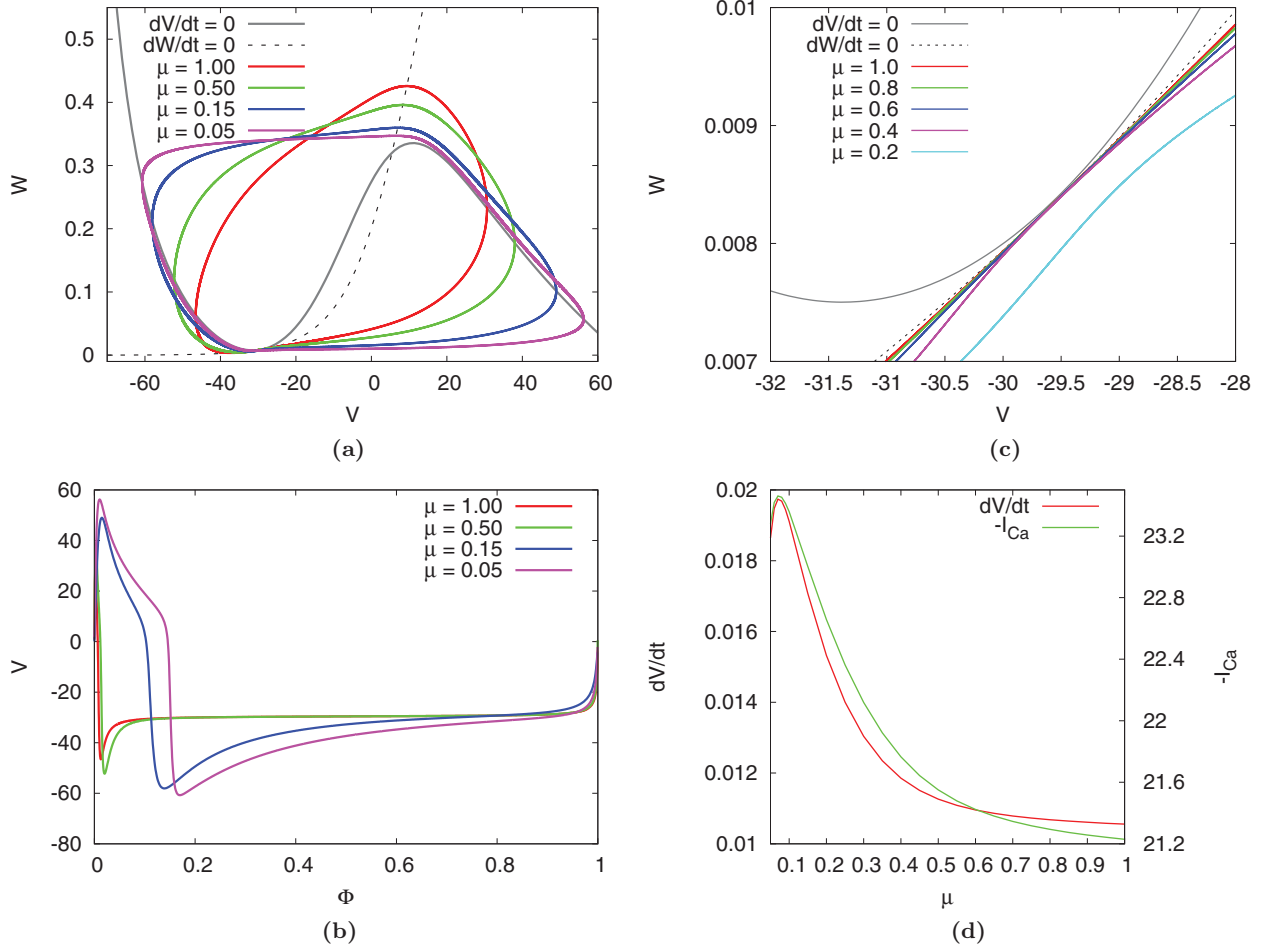


FIG. 2. (Color online) Trajectories on V - W plane diagrams and time evolutions of membrane potential for the ML model with $I = 39.7$ influenced with a temperature scaling factor μ . (a) The whole nullclines of $dV/dt = 0$ (a solid line) and $dW/dt = 0$ (a broken line) depicted on the V - W plane. In (b), the temporal duration between points indicates a velocity of V . The V motion on the active or inactive phases gradually becomes slower. Φ is a variable normalized by periodicity. (c) The V - W plane (a) is scaled up toward the saddle-node bifurcation point. (d) Plots of μ on dV/dt and $-I_{Ca}$.

Analyzing the membrane potential dynamics, in particular, hyperpolarization, we shall explain the thermal effects of a firing frequency. In Fig. 3(a), the right-most intersection of the two nullclines, $(V_e, W_e) \sim (5.47, 0.32)$, is shown to analyze its stability as μ changes in the range of $[1, 2]$. The stability analysis tells us that for $\mu = 2$ the Jacobian calculated at this unstable equilibrium has a complex eigenvalue, so that the trajectory spirals away toward the stable limit cycle.

However, when $\mu = 0.1$, the equilibrium changes from an unstable spiral to an unstable node. The trajectory is then quickly attracted to the limit cycle without any spiral [Fig. 3(a)]. Physiologically, when the temperature is high, the potassium channels can open and close very rapidly. As soon as the voltage hyperpolarizes a little from its high plateau value, the potassium channels close immediately, which in turn allows the voltage to depolarize again. The depolarization in turn rapidly opens the potassium channels, which hyperpolarizes the voltage, resulting in the oscillation as seen in Figs. 3(a) and 3(b). Such oscillation seems to be inhibited for lower temperatures with slower potassium channel openings. Nevertheless, the firing frequency is higher, as shown in Fig. 3(b). In fact, the firing frequency around the

temperature corresponding to $\mu = 0.15$ is highest and those for other temperature values are lower, as we show explicitly later.

B. Frequency versus current relationship

We investigate a systematic distribution of the firing frequency in terms of I and μ [Fig. 4(a)]. We then show the f - I curves [Fig. 4(b)] as well as the frequency-temperature relations [Fig. 4(c)]. This confirms an increased firing frequency for smaller μ around the I value where the saddle-node bifurcation occurs, as mentioned in the previous section.

Figure 4(a) shows a systematic scheme of firing frequencies for both μ and I . We obtain typical class I f - I curves, at least when $\mu > 0.2$. When μ decreases from 0.2, the f - I curves look like class II, but the firing frequency increases from 0 at I_c with the logarithmic approximation of $1/[-\ln(I - I_c)]$ [as shown in Fig. 4(b)] [18–20]. In Fig. 4(b), I_c represents the critical point of I . The logarithmic curves may be class I, but we will need to discuss more carefully whether the curves are class I or class II, being mindful of the PRC analysis described below.

Figure 4(c) shows changes of the firing frequency for μ at a fixed value of I . When I is less than the saddle-node

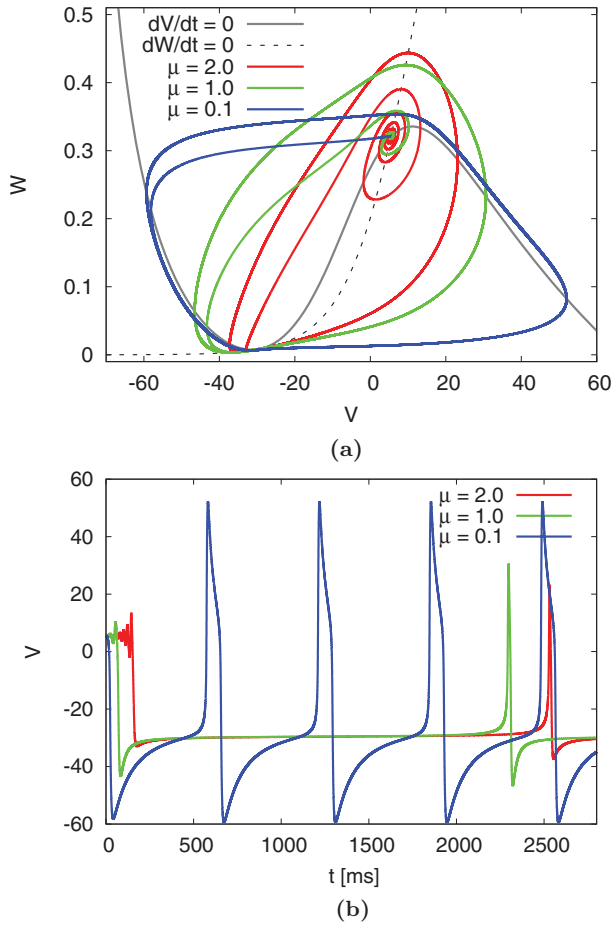


FIG. 3. (Color online) Simulation results of the hyperpolarization process in the ML model. (a) Trajectories, which are controlled with three different temperature scaling factors $\mu = 2.0, 1.0,$ and $0.1,$ are drawn when they start near an unstable fixed point on the V - W phase plane. (b) Such hyperpolarization demonstrations also shown with time evolutions of the membrane potential. Here $I = 39.7.$

bifurcation point I_{sn} , the firing frequency is 0 for $\mu > \mu_c$, or it increases for $\mu < \mu_c$. The mechanism for increasing the firing frequency for μ below μ_c has already been mentioned in the previous section.

C. Phase response curve

In Sec. II-B, f - I and f - μ relations have been revealed with the ML model in the saddle-node (SN) bifurcation with changes of I . Also, let us survey systematic changes of the PRC, Z_V , to find their relation to the frequency curve [Fig. 5(a)]. In such a survey, the logarithmic f - I curve for small μ [see Figs. 5(b) and 5(c)] and the f - μ curve at I around the SN bifurcation point [Figs. 5(d) and 5(b)] must be fascinating, particularly because the PRC shift of type I to type II on the class I f - I curve [Figs. 5(d) to 5(e)] or the type II PRC maintained on the class II f - I have so far been studied [37]. The PRCs are computed using a phase-reduction method (see Appendix).

We study how I affects the phase response curve, referring to the f - I curve for $\mu = 0.2$ in Fig. 5(b). When I is just a little larger than I_c , the PRC takes a type-I-like type II. Its

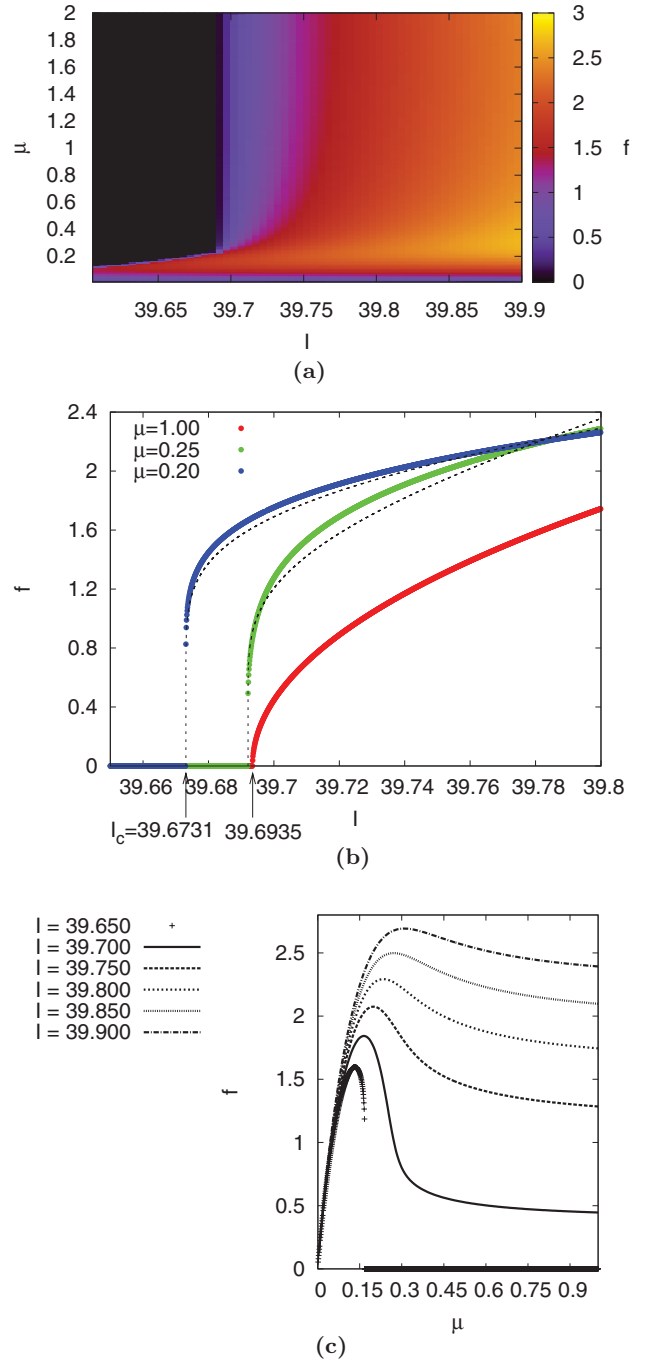


FIG. 4. (Color online) Temperature-scaling-factor-dependent firing frequency f vs current (I) relationship for the ML model. (a) An I - μ diagram for f . (b) Different f - I curves with $\mu = 1.0, 0.25,$ and $0.20.$ Broken lines show functions of f as $I - I_b$, where I_b is near the bifurcation. (c) f - μ curves at fixed I .

PRC is slightly different from the well-known type II form so that the positive peak of the PRC is extremely high but the negative region is also apparently visible. When $\mu = 0.2$ and I is far from I_c , the peak is drastically reduced; correspondingly, the action potential duration is gradually extended [Fig. 5(f)], and one obtains the typical type II form as shown in Fig. 5(c). This is independent of I for further smaller values of μ .

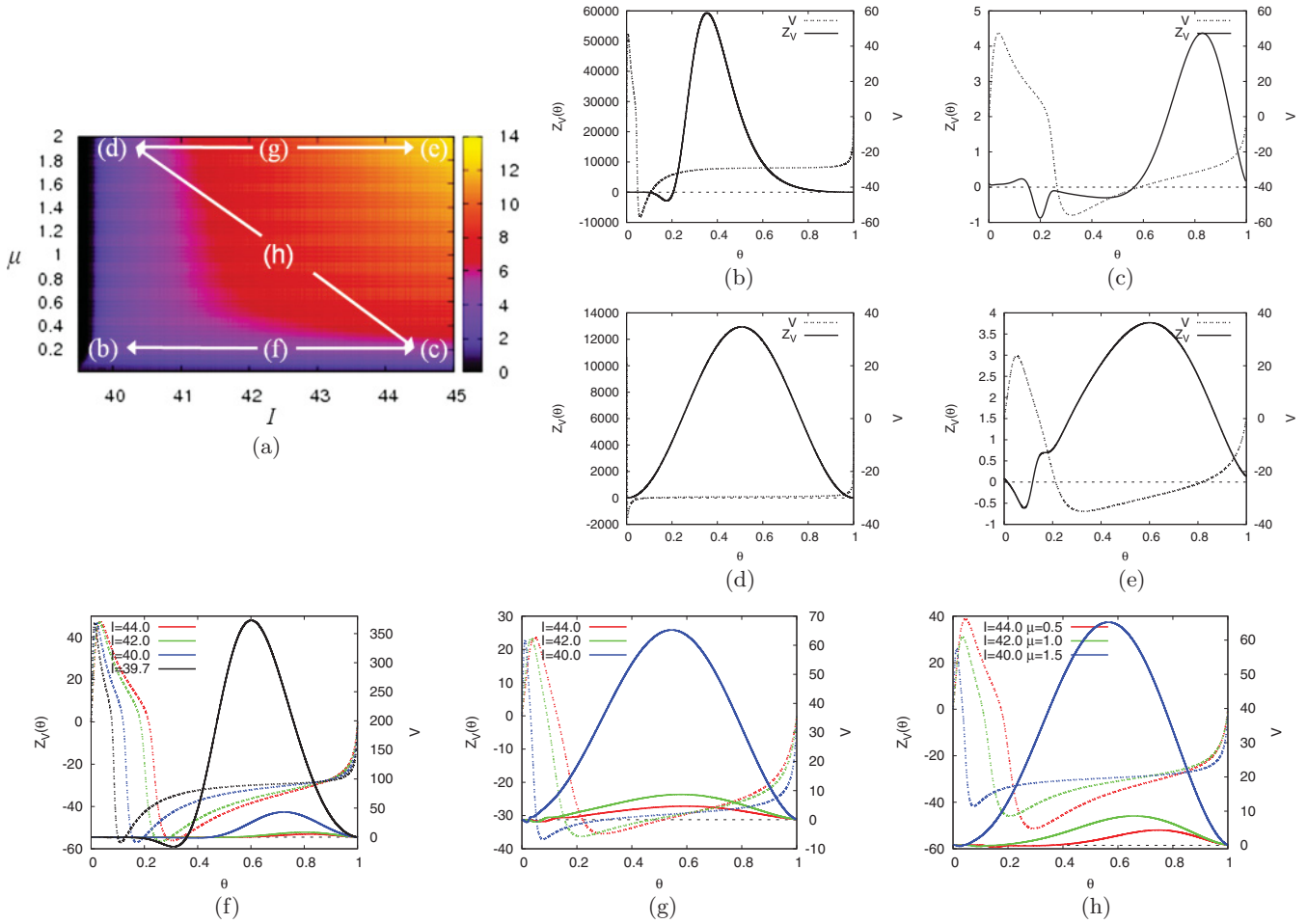


FIG. 5. (Color online) (μ, I) -dependent PRCs for the class I type ML model, corresponding to the membrane potential dynamics. (a) represents a color map for a firing frequency, in terms of I and μ . (b) to (e) show PRCs and membrane potential dynamics. (b) $I = 39.6732$ and $\mu = 0.2$. (c) $I = 45.0$ and $\mu = 0.2$. (d) $I = 39.694$ and $\mu = 2.0$. (e) $I = 45.0$ and $\mu = 2.0$. (f) to (h) demonstrate continuous changes of PRCs and membrane potentials (V) with I and/or μ in the class I type ML model. (f) and (g) show PRCs and V at different values of I when $\mu = 0.2$ and $=2.0$, respectively. (h) PRCs and V vary with changes of both I and μ . Here the solid lines are the PRC curves while the broken lines are for membrane potential dynamics.

For f - I curves for $\mu = 2.0$, we simulate changes of the PRC in a gradual increase of I from the SN bifurcation I_{sn} . The typical type I PRC around $I = I_{sn}$ [Fig. 5(d)] is obtained. However, as shown in Fig. 5(g), the positive peak goes down while the spike duration is longer to expand the negative PRC region, giving the PRC at $I = 45.0$ [Fig. 5(e)], which is slightly different from that for a typical type II PRC. In Fig. 5(h), we show PRC shifts from the typical type I to the typical type II form with changes of both I and μ .

We show an additional result for μ -modulated PRC shape changes, which is drawn as a color map in Fig. 6. The PRC is potentially related to derivations of synchronized solutions found in a pair of coupled neuronal oscillators. Especially, depending on the dynamical influence of the synapses, we can easily predict which type of synchronization is obtained: for example, completely simultaneous or out-of-phase firings of the two neurons. In Fig. 6(a) for $I = 39.7$, we can see that the PRC takes almost positive values for larger μ . However, when μ is significantly less than 0.2, it can have a region showing obvious negative values as well, which is widely extended with an increase of I to 45.0 as shown in Figs. 6(b)–6(d).

In this brief conclusion, we have shown the following: (1) Around the SN bifurcation of I , the firing frequency for smaller μ is higher, compared to the ones for larger μ . Being far from the SN bifurcation point (at least $I > 40.0$), the firing frequency is monotonically higher in increments of μ . (2) Around the critical value of I in a logarithmic f - I curve for small μ , we have obtained a type II PRC, although some type I partially remains. For much smaller μ , the PRC becomes type II independent of values of I .

III. COMPUTATIONAL ANALYSIS OF SYNCHRONIZATION TRANSITION

In the previous section, by systematically surveying f - I curves and the PRCs, we have found some unique firing properties. It may be very interesting and meaningful to argue how such firing properties influence the synchronization transition even in a pair of neurons.

To study such influence of the firing properties on synchronization transition, the phase-reduction method is employed for describing equations consisting of phase degrees of

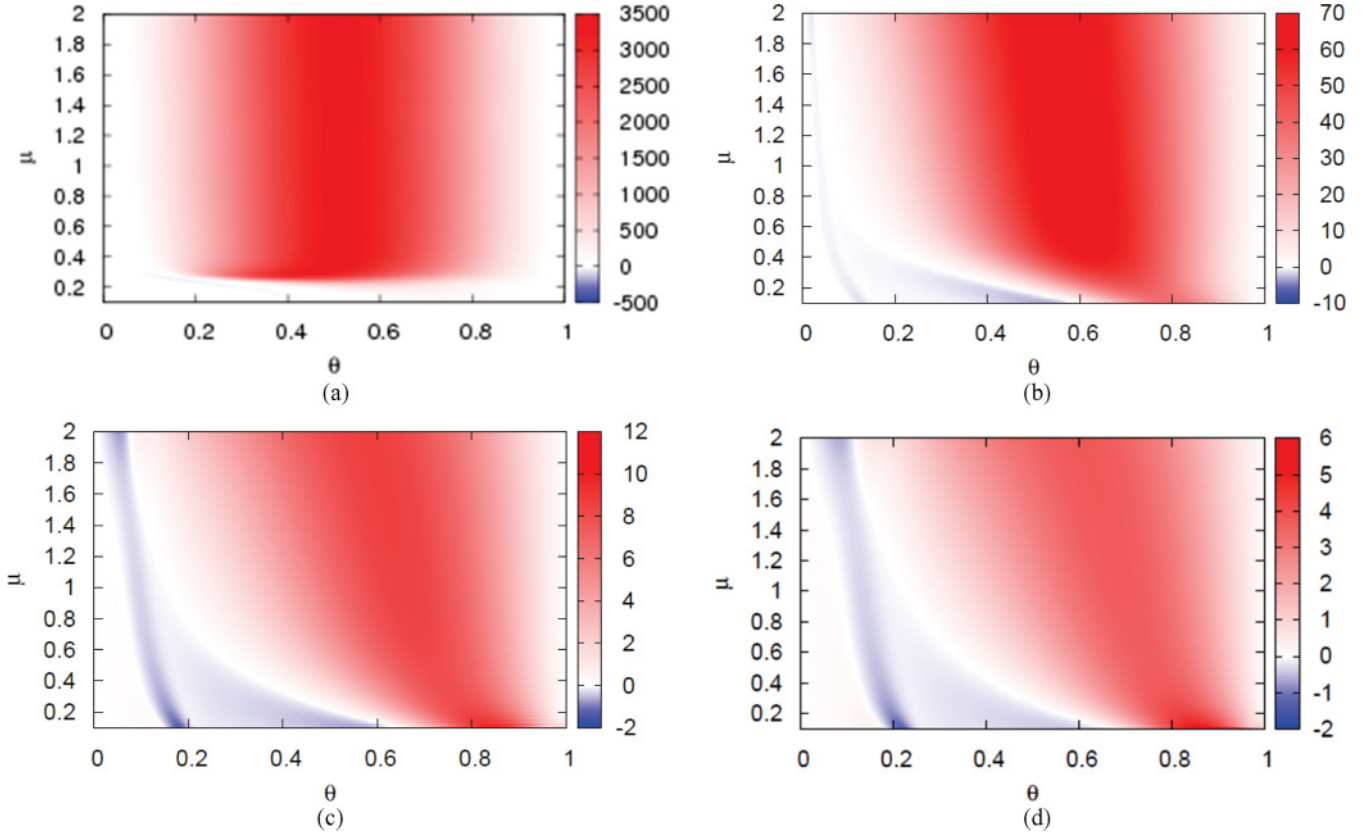


FIG. 6. (Color online) PRC (Z_V) shape shifts in a range of $\mu = 0.1$ to 2.0 . Red and blue represent, respectively, positive and negative values of Z_V . (a) $I = 39.7$, (b) $I = 40.0$, (c) $I = 42.0$, and (d) $I = 45.0$.

freedom from a pair of coupled ML neurons [Appendix]:

$$\frac{d\mathbf{x}_i}{dt} = \mathbf{F}(\mathbf{x}_i) + \epsilon s_{\bar{i}}, \quad i = 1, 2, \quad (5)$$

where \bar{i} represents a counterpart of the i th neuron. $\mathbf{x}_i = (V_i, W_i, s_i, h_i) \in \mathbb{R}^4$. $\mathbf{F}(\mathbf{x}_i)$ is a baseline vector field represented by Eqs. (1)–(4). The excitatory synaptic coupling $\epsilon s_{\bar{i}}$ is weak to give straightforward insight into the dynamical relation of the synchronous behavior in the two neurons to their PRCs. So, we have to notice that the synaptic couplings used here are slightly different from the physiologically rigorous case with the synaptic reversal potential term.

The phase equation gives us an explanation for how the PRC is related to synchronized solutions ϕ as well as for the stabilities (Fig. 7). Such stabilities of synchronized solutions are analyzed in term of α , I , as well as μ (Figs. 8 and 9). Results of bifurcations of ϕ for μ enable us to show an intriguing phenomenon that a two-neuron system becomes synchronized by sinusoidal temperature modulation (Figs. 10 and 11). We will give brief discussions about the mechanisms regarding how the specific firing properties mentioned in Sec. II affect such sinusoidal-wave-tuned synchronization.

A. Linear stability analysis

In the phase-reduction method, phase equations are given as follows:

$$\frac{d\phi}{dt} = H_2(\phi) - H_1(-\phi) \equiv \Gamma(\phi), \quad (6)$$

where $\phi = \theta_1 - \theta_2$ denotes the phase difference between the two neurons. $\Gamma(\phi)$ is expressed as an average interaction function ϕ as defined in Appendix.

A linear stability analysis for Eq. (7) provides us with a simple explanation for how the stationary synchronous states arise in a two-neuron system. For instance, let us consider the case $\alpha = 1/\tau_{\text{syn}} = 1$, based on a theoretical assumption that the PRC is a significant factor for converging to the stationary synchronous states. We compute the relevant $H_i(\phi)$ function to obtain $\Gamma(\phi)$ without a loss of PRC properties [Figs. 7(a) and 7(b)]. Synchronized solutions are then represented as fixed points, ϕ_0 , being satisfied with the stationary condition $\Gamma(\phi_0) = 0$. The in-phase and antiphase synchronized solutions are defined, respectively, as $\phi_0 = 0$ or 1 and $\phi_0 = 0.5$. The synchronized solutions are stable if $\Gamma'(\phi_0) < 0$, while they are unstable if $\Gamma'(\phi_0) > 0$ [Figs. 7(a) and 7(b)].

Now, we will show how a temperature-scaling factor μ influences the scheme of synchronization of oscillations with respect to $\alpha = 1/\tau_{\text{syn}}$ by a stability analysis for $\Gamma(\phi)$. Numerical calculations are used for all results obtained using the linear stability analysis for the phase equation. These results are in agreement with numerical simulations, conducted with a fourth-order Runge-Kutta method for the ML models [Figs. 7(c) and 7(d)].

B. Synchronization transition

We analyze the stability of synchronization solutions, in terms of α , μ , and I . The results of such a stability analysis

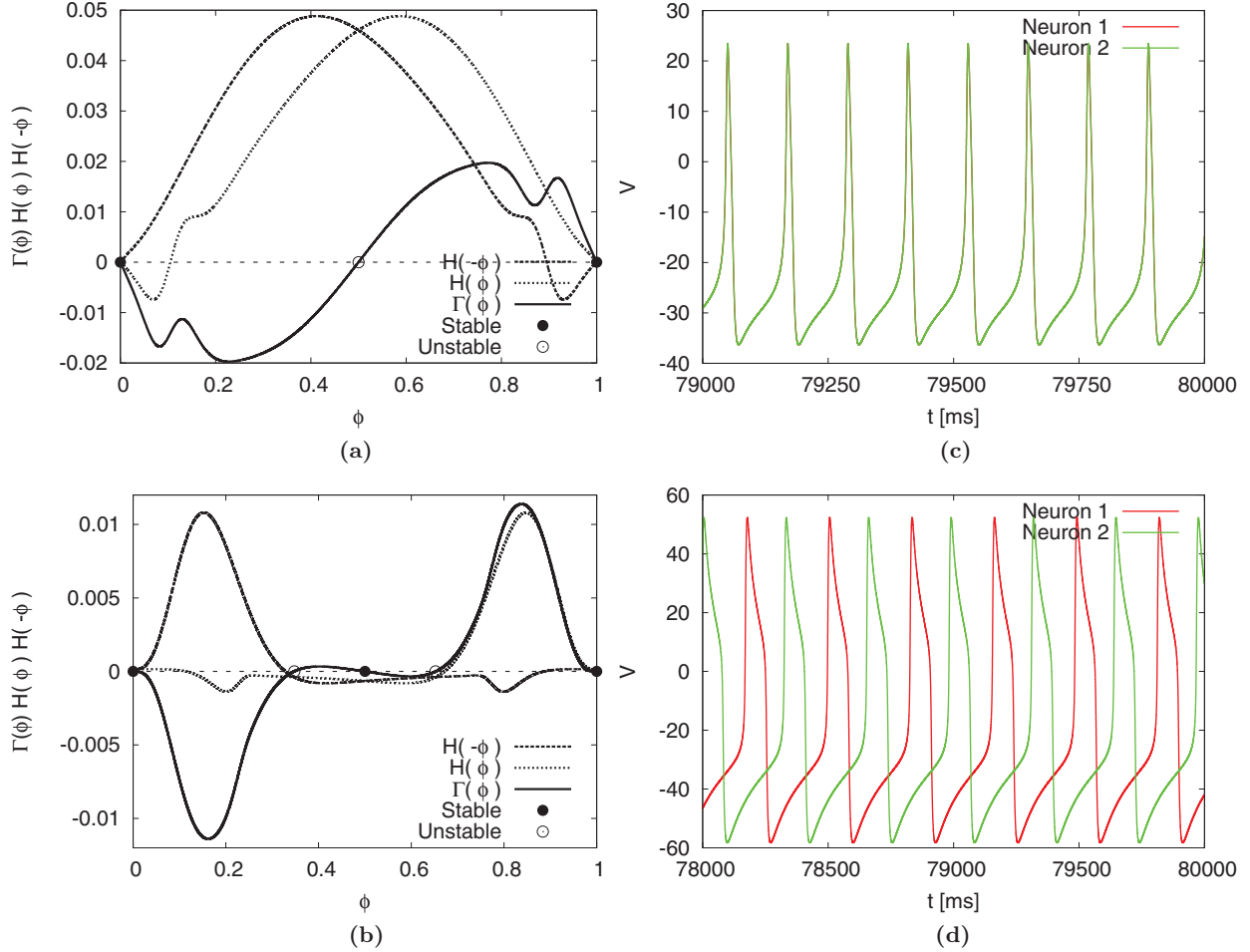


FIG. 7. (Color online) Linear stability analysis for synchronous states between two neurons. $H_1(\phi)$, $H_2(-\phi)$, and $\Gamma(\phi)$ in Eq. (7) are calculated with parameters of $\alpha = 1/\tau_{\text{syn}} = 1.0$ and $I = 45.0$. (a) $\mu = 2.0$ and (b) $\mu = 0.1$. Filled circles designate stable solutions while open circles designate unstable solutions. Two arrows show convergence directions to stable stationary synchronous states, which are demonstrated on numerical simulations in (c) and (d).

are shown in Fig. 8, with $I = 39.7, 40.0, 42.0$, and 45.0 and $\mu = 0.01, 0.05, 0.1, 0.5, 1.0$, and 2.0 . In Fig. 8, bifurcations of ϕ are drawn in an α range of $(0, 1]$ where red and green lines, respectively, mean unstable and stable states of ϕ . By finding common dynamical properties for synchronization transition in Fig. 8, we also show phase difference bifurcations in a μ range of $(0, 2]$ [Fig. 9].

We can figure out a common synchronization transition when μ varies at a fixed amplitude of I , although Fig. 8 shows very complicated synchronization transitions appearing in the bifurcation diagram. The case of $I = 45.0$ is the most understandable simulation result. In this case, we find a supercritical pitchfork bifurcation at $\phi = 0.5$ as well as a subcritical pitchfork bifurcation at $\phi = 0$ redefined with $\phi = [-0.5, 0.5]$ when μ decreases from 2 to 1. The corresponding stable and unstable branches are connected at arbitrary values of α and ϕ . The subcritical pitchfork bifurcation at $\phi = 0$ is annihilated so that there is only a supercritical pitchfork bifurcation. When μ decreases to 0.5, a new supercritical pitchfork bifurcation appears at a smaller α . The two bifurcation points coalesce (not shown here), so that each stable branch is combined with the counterpart to shift the branches to $\phi = 0$ or 1 as in the cases of $\mu = 0.1$ and 0.05 . Finally, for $\mu = 0.01$, we can see

a new subcritical pitchfork bifurcation at $\phi = 0.5$ for large α , with coexistence of $\phi = 0, 0.5$, and 1 . It is noticed here that the subcritical pitchfork bifurcation does not rely on values of I .

The results of the μ -modulated synchronization transition give another interpretation of the μ -modulated bifurcation of ϕ in Fig. 9, where $\alpha = 1$ and $I = 45.0$. In this case, a subcritical pitchfork bifurcation is computed around $\mu = 0.1$. When μ become gradually larger, stable in-phase and unstable antiphase synchronizations appear. Such synchronization transitions are qualitatively independent of the value of I . Here we mention the reason in the case of $\alpha = 1.0$: PRC shapes are qualitatively similar to their related H functions. It makes sense that the PRC shape is directly related to the computation of synchronization solutions. Also, Fig. 8 gives us straightforward expectations to find another ϕ bifurcation diagram for μ , except for $I = 45.0$.

C. μ -sinusoidal tuned synchronization

We study effects of the following firing properties on synchronization or desynchronization in a numerically simulated two-neuron system: (1) subcritical pitchfork bifurcation of ϕ for μ and (2) f - μ curves around the saddle-node bifurcation point of I .

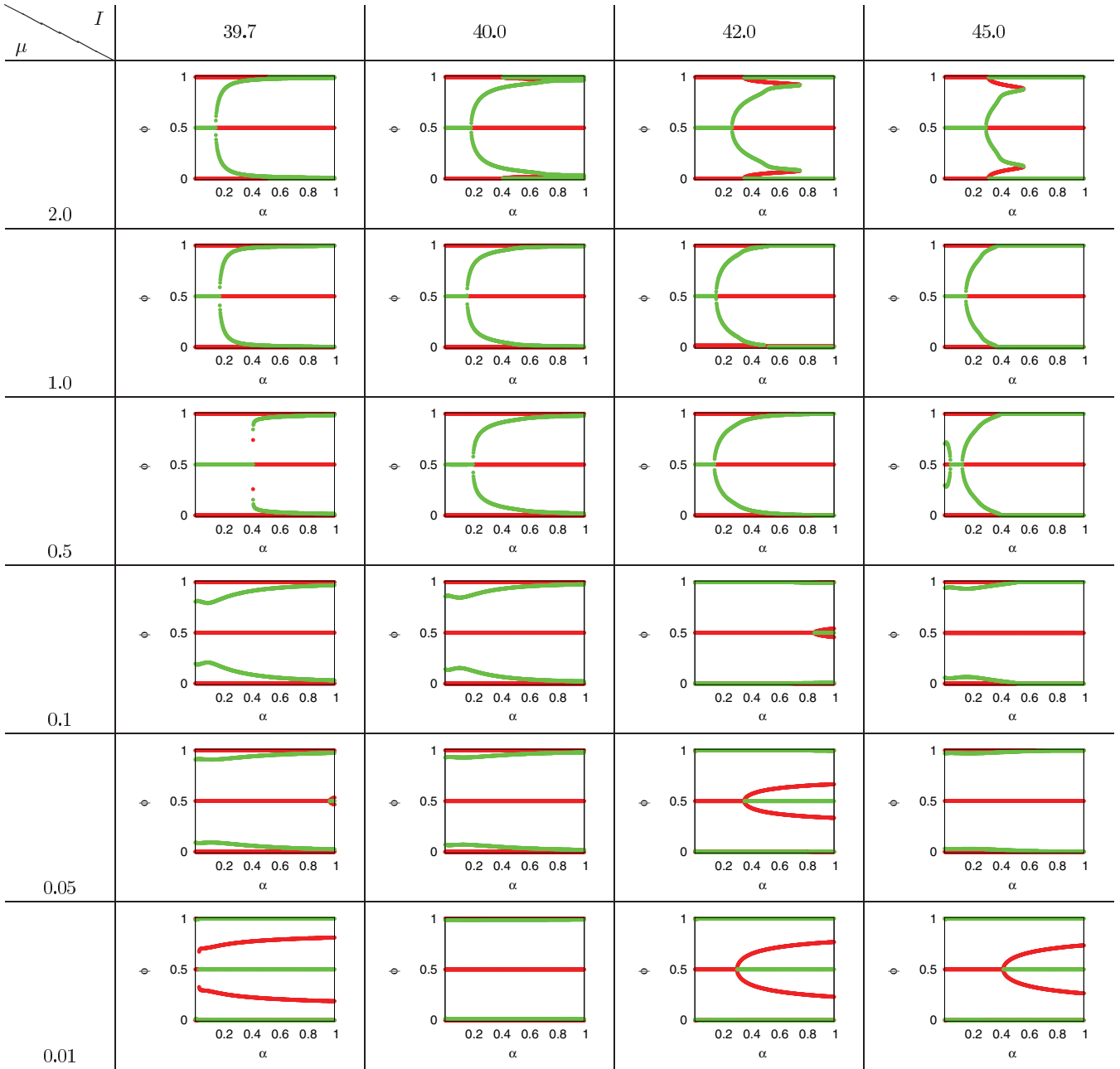


FIG. 8. (Color online) (I, μ) -modulated change of the bifurcation diagram for phase differences ϕ in the range of $\alpha = (0, 1]$. Here $I = 39.7, 40.0, 42.0,$ and 45.0 while $\mu = 2.0, 1.0, 0.5, 0.1, 0.05,$ and 0.01 . Red and green lines, respectively, show that the phase differences are in the unstable and stable states.

In such numerical simulations, μ in the ML model is given by

$$\mu(t) = 0.01 + \mu_1(t) [1 - \cos(2\pi f_1 t)] + \sigma \xi_i(t), \quad (7)$$

$$\mu_1(t) = \begin{cases} 0.01, & \text{if } t < t_s, \\ h_1, & \text{else,} \end{cases} \quad (8)$$

where i is the neuron index. $\xi_i(t)$ is white Gaussian noise such that $\langle \xi(t) \rangle = 0$ and $\langle \xi_i(t) \xi_j(t') \rangle = 2\delta_{ij} \delta(t - t')$, where $\langle \dots \rangle$ denotes averaging over ξ , and δ is the Dirac delta function. We call the constant σ the noise intensity. Here $\sigma = 0.01$ is fixed in all numerical simulations because the noise intensity does not affect the synchronization-desynchronization process. h_1 is the

amplitude of the sinusoidal wave. The frequency of the sine wave, f_1 , is set with 2, 3, and 4 Hz. $t_s (= 2.5)$ s is a switch time for incrementing the amplitude. It should be noticed that we add additional white Gaussian noise to the membrane potential dynamics, whose intensity is 0.02. Let the initial states of two neurons be in the antiphase synchronization state. The synaptic time constant is 1 ms.

Let us simulate synchronous phenomena in two coupled neurons, in which μ is a sine wave with $f_1 = 2$ (or 3). When $I = 39.7$, the two neurons become synchronized in phase, unrelated to the sine-wave modulation at $h_1 = 0.02$ (or 0.06) [Fig. 10(a)]. When h_1 becomes gradually higher, the two neurons become desynchronized once. However,

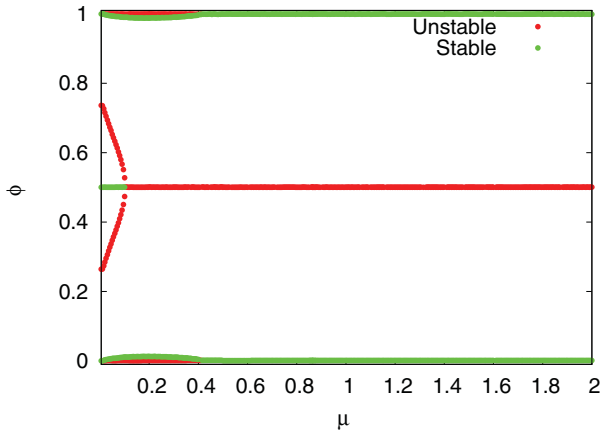


FIG. 9. (Color online) A bifurcation diagram for ϕ in $\mu = (0,2]$. We set up with $\alpha = 1.0$ and $I = 45.0$.

for much higher h_1 , synchronization tuned with 1:1 to the sinusoidal-wave period are regenerated [see Fig. 10(b)]. In the case of $f_1 = 4$, when the value of h_1 is larger, an asynchronous state is transited to simultaneous firings per $2f_1$ [Fig. 10(c)].

In the range of I , [40.0,45.0] (namely, far from the saddle-node bifurcation point), we have found synchronization tuned with 1:1 to the sine-wave period f_1 in a colored area [see Fig. 11(a)]. The two neurons are in the asynchronous state outside the colored area, because increasing h_1 makes dV/dt become unadaptive to f_1 .

The sinusoidal μ -tuned synchronization can be explained using the following dynamical mechanisms: (1) subcritical pitchfork bifurcation of μ for ϕ and (2) a specific f - μ curve around the SN bifurcation point. The first mechanism gives a suitable reason for why synchronizations as shown in Fig. 10 are simulated. When $h_1 = 0.02$ for $f_1 = 2.0$, μ is larger than the bifurcation point so that the pair system is in a simultaneous firing state without any difficulties, regardless of the sine-wave period. In addition, the second mechanism gives us a reasonable statement about f_1 -tuned synchronization: The h_1 range, observed in the f_1 -tuned synchronization, becomes rapidly wider when I decreases [Fig. 11(a)]. This can be considered to be because the firing frequency f remains constant for small I , as seen in Fig. 4(c), so that the two neurons can be synchronized easily with the period of the sine wave. For larger I , a monotonic increase of f with an increment of μ causes the difference with respect to f_1 to be big. f_1 -tuned synchronization can be observed but with great difficulty.

IV. DISCUSSION AND CONCLUSION

In this work, we studied the μ -dependent f - I curve accompanied by continuous changes of the PRC shape [Fig. 5]. We found two unique firing properties for small μ : (1) a peak of firing frequency and (2) type II PRCs on a logarithmic class I f - I curve. The firing properties could not be shown, even though a mechanism for the onset of repetitive firing in the f - I curve was revealed with analyses on stabilities of equilibria and the relevant bifurcation structure [18–20]. However, to find two firing properties, a rigorous analysis of the trajectories and PRC derivations by the phase-reduction method is necessary.

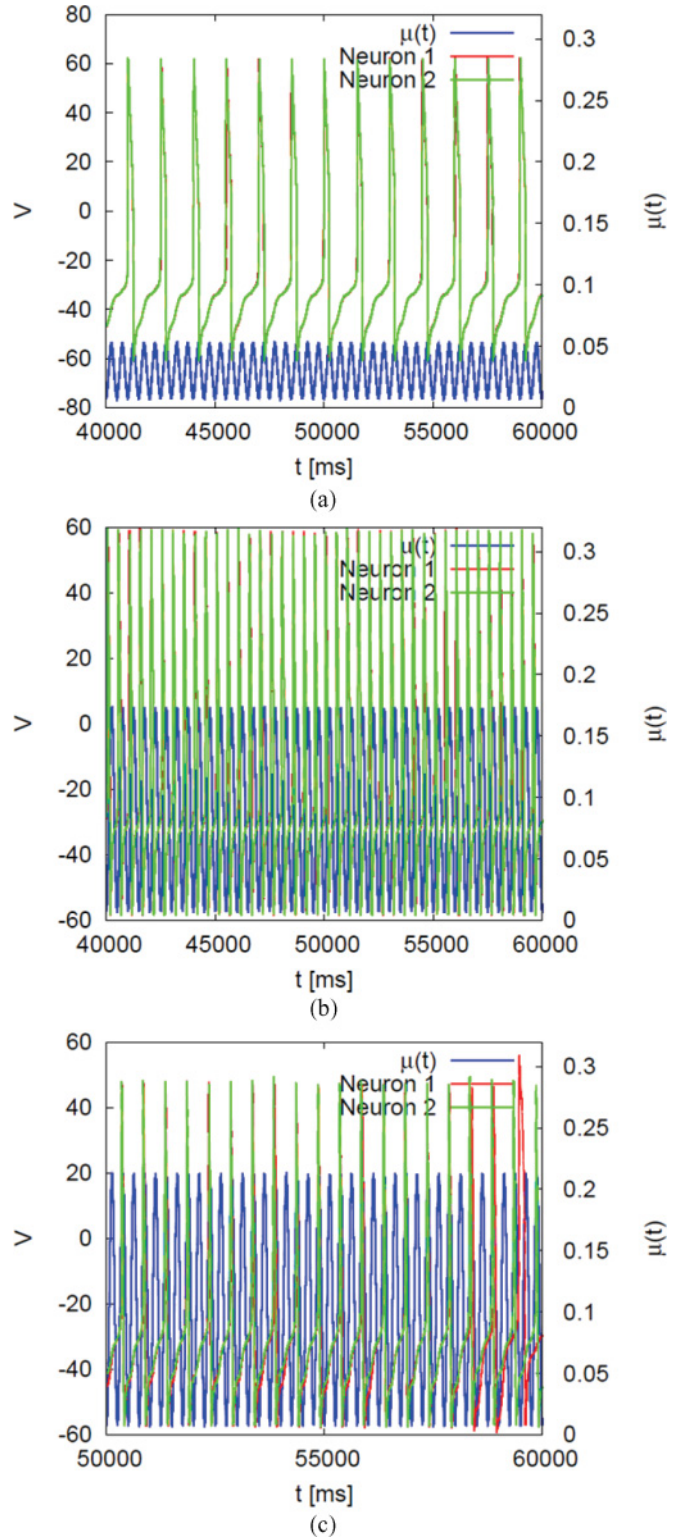


FIG. 10. (Color online) Synchronization with or without sine modulations of μ . (a) Simultaneous firings, not accompanying the μ sine wave. Here $f_1 = 2$ and $h_1 = 0.02$. (b) Simultaneous firings tuned with the sine wave, where $h_1 = 0.08$ for $f_1 = 2$. (c) Synchronization occurring every two periods for $f_1 = 4$ and $h_1 = 0.12$.

The first firing property has not been reported thus far. It is still unclear whether such a property has been observed in experiment, because the experiments [21–23] and

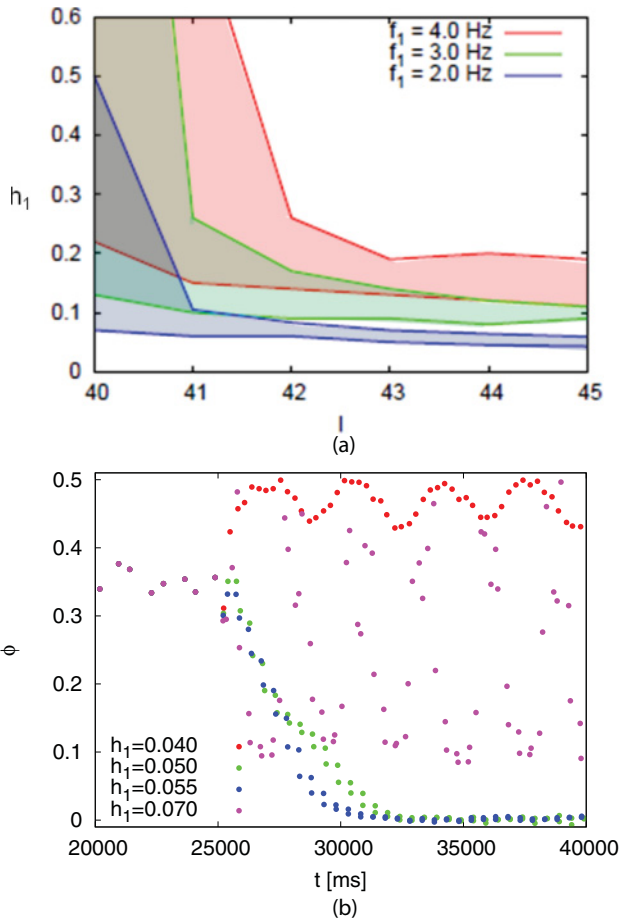


FIG. 11. (Color online) Synchronization with sine-wave modulations of μ . (a) h_1 - I diagrams for synchronization states. (b) Synchronization at different values of h_1 after switching the sine-wave amplitude higher.

model studies [24] found only a monotonically descending frequency for lower temperature. We will have to await reporting of our observations of ascending frequency for lower temperature.

However, if a constant low frequency for higher temperature is observed, this may support partially an ascending frequency for lower temperature. For this support, it is necessary to confirm that neurons used in the experiments take the type I PRC. As shown in Fig. 5(d), the type I PRC takes highly positive values dominantly on the phase. This implies that dV/dt is extremely small under the normalization condition PRC and dV/dt (see the Appendix). Thus, we can easily expect a low frequency for higher temperature. Since it has already been shown in physiological experiments that layer V pyramid cells in the rat motor cortex tend to exhibit a type I [38,39] form, we may observe increased (or decreased) frequencies for such neurons for lower (or higher) temperature.

The second firing property, type II PRCs for smaller μ , independent of I , indicates that the logarithmic class I f - I curve would rather be class II. This is however no more than an indication. To verify the I -independent PRCs of type II, we will have to clarify some quantitative relationship of the f - I curve to the PRC. Let us consider again a definition for a

phase equation derived with the phase-reduction method. The H function involving the PRC in the phase equation presents expansion and contraction of the firing frequency. This implies that the PRC may be related to the slopes of the f - I curves. In any case, if we can formulate a relationship between the PRC and the f - I curve, we will be able to address whether the logarithmic class I f - I curve is class II.

Reconsideration regarding how Q_{10} is dealt with is an urgent task for observing two firing properties in a real physiological experiment. Let us imagine neuronal activities in the homoiotherm's brain. We will have to realize dramatic changes of neuronal activities with a narrow range of temperature. But, as mentioned in Sec. I, Q_{10} has so far been set up as 3 or smaller. The available environmental temperature range was also very low. Neurons in cold-blooded animals were often employed for physiological experiments on the effects of temperature on neuronal activity.

In recent years, some researchers have recorded high Q_{10} ($=19$) for calcium-channel gating in experiments [40]. If high temperature coefficients can be recorded for other channel gates such as sodium and potassium, we can also expect to discover a temperature dependence for firing properties, in particular, increased frequency and a logarithmic frequency-current relationship for small μ .

If we can control a narrow temperature range in a real physiological experiment, observations of neuron activities synchronized by temperature oscillatory stimulation may also be realized. This is because experiments on Physarum polycephalum have already shown that the activities can be controlled with temperature oscillatory stimulation [41,42]. Since, in this work, mechanisms on temperature-sine-wave-modulated synchronization were explained by another dynamical property of f - μ curves and phase difference bifurcations for μ , such studies are very computational. If such experiments can be done using neurons in homoiotherms, our results are not only computational but also more neuroscientific and provide intriguing ideas for experiments.

In conclusion, we have systematically studied synchronization transition in a pair of synaptically coupled neuronal oscillators of the ML type, in terms of μ and I . This study is based on phase-plane analysis for membrane potential dynamics as well as on linear stability analysis using the one-dimensional oscillator reconstructed by a phase-reduction method. We then showed a specific temperature dependence of the firing frequency and the phase-response curve. We also found qualitatively common temperature-modulated synchronization transitions, independent of I . Mechanisms for such synchronization transitions give us explanations for mechanisms on synchronization phenomenon tuned with sinusoidal temperature modulation.

ACKNOWLEDGMENTS

Y.D.S. was supported by the Grant-in-Aid for Young Scientists (B) No. 22700237. A.I. was supported by the Grant-in-Aid for JSPS Fellows No. 20.9513. H.C. was supported by Grant-in-Aid for Scientific Research (C) No. 23500267. The authors thank Natsume and Ikegaya for fruitful and active discussions.

APPENDIX: PHASE-REDUCTION METHOD

The phase-reduction method is briefly reviewed. For a detailed derivation the reader is referred to [43,44]. Suppose we have a pair of coupled identical ML oscillators. When the synaptic coupling is weak, this method should be applied to

$$\frac{d\mathbf{x}_i}{dt} = \mathbf{F}(\mathbf{x}_i) + \epsilon \mathbf{G}(\mathbf{x}_i, \mathbf{x}_{\bar{i}}). \quad (\text{A1})$$

Let $\mathbf{x}_p^{(i)}(t)$ denote a stable T_p -periodic solution for the uncoupled dynamics,

$$\frac{d\mathbf{x}_p^{(i)}}{dt} = \mathbf{F}(\mathbf{x}_p^{(i)}), \quad (\text{A2})$$

where $\mathbf{x}_p^{(i)}(t + T_p) = \mathbf{x}_p^{(i)}(t)$. Then a stable solution for Eq. (A1) is approximated as

$$\mathbf{x}_i(t) = \mathbf{x}_p^{(i)}[t + \tau_i(t)] + \epsilon \mathbf{u}_i[t + \tau_i(t)] + O(\epsilon^2), \quad (\text{A3})$$

where $\tau_i(t)$ means a small perturbation in the phase direction on the periodic orbit. $\epsilon \mathbf{u}_i[t + \tau_i(t)]$ denotes the orbital deviation to the periodic orbit $\mathbf{x}_p^{(i)}(t)$. Substituting Eq. (A3) into Eq. (A1) and expanding both sides into a Taylor series leads to

$$\begin{aligned} & \left[\dot{\tau}_i(t) \frac{d\mathbf{x}_p^{(i)}(q)}{dq} + \epsilon \frac{d}{dq} \mathbf{u}_i(q) \right]_{q=t+\tau_i(t)} \\ &= \frac{\partial \mathbf{F}(\mathbf{x}_p^{(i)}[t + \tau_i(t)])}{\partial \mathbf{x}} \mathbf{u}_i[t + \tau_i(t)] \\ &+ \epsilon \mathbf{G}(\mathbf{x}_p^{(i)}[t + \tau_i(t)], \mathbf{x}_p^{(\bar{i})}[t + \tau_{\bar{i}}(t)]) + O(\epsilon^2). \end{aligned} \quad (\text{A4})$$

Here we have used the fact that $\dot{\tau}_i(t) = O(\epsilon)$. In the perturbed oscillator, the orbital deviation vector $\mathbf{u}_i(t) = \mathbf{x}_i(t) - \mathbf{x}_p^{(i)}(t)$ evolves as

$$\dot{\mathbf{u}}_i(t) = \frac{\partial \mathbf{F}(\mathbf{x}_p^{(i)}(t))}{\partial \mathbf{x}} \mathbf{u}_i(t) + O(\epsilon). \quad (\text{A5})$$

The vector $\mathbf{Z}(t)$ is tangent to the periodic orbit $\mathbf{x}_p^{(i)}(t)$, which is the unique solution to

$$\frac{d}{dt} \mathbf{Z} = - \left[\frac{\partial \mathbf{F}(\mathbf{x}_p)}{\partial \mathbf{x}} \right]^T \mathbf{Z}, \quad (\text{A6})$$

where the normalization condition $\mathbf{Z}^T \cdot [d\mathbf{x}_p/dt] = 1$ is enough for every t and T means a transpose. Equation (A1) is then reduced to the evolution equation for τ_i :

$$\dot{\tau}_i(t) = \mathbf{Z}[t + \tau_i(t)]^T \cdot \mathbf{G}(\mathbf{x}_p^{(i)}(t + \tau_i), \mathbf{x}_p^{(\bar{i})}(t + \tau_{\bar{i}})). \quad (\text{A7})$$

Introducing phase variables defined by $\theta_i = (t + \tau_i)/T_p$, we can rewrite Eq. (A7) as

$$\frac{d\theta_i}{dt} = \frac{1}{T_p} + \frac{1}{T_p} \tilde{\mathbf{Z}}(\theta_i)^T \cdot \mathbf{G}(\tilde{\mathbf{x}}_p^{(i)}(\theta_i), \tilde{\mathbf{x}}_p^{(\bar{i})}(\theta_{\bar{i}})), \quad (\text{A8})$$

where $\tilde{\mathbf{x}}_p^{(i)}(\theta_i) = \mathbf{x}_p^{(i)}(t + \tau_i)$ and $\tilde{\mathbf{Z}}(\theta_i) = \mathbf{Z}(t + \tau_i)$. The phase difference of the two oscillators, $\phi(t) = \theta_2(t) - \theta_1(t)$, obeys

$$\frac{d\phi(t)}{dt} = \hat{H}_2(\theta_2, -\phi) - \hat{H}_1(\theta_1, \phi), \quad (\text{A9})$$

where the function $\hat{H}_i(\theta_i, \phi)$ is defined by

$$\hat{H}_i(\theta_i, \phi) = \frac{\epsilon}{T_p} \tilde{\mathbf{Z}}(\theta_i)^T \cdot \mathbf{G}(\tilde{\mathbf{x}}_p^{(i)}(\theta_i), \tilde{\mathbf{x}}_p^{(\bar{i})}(\theta_i + \phi)). \quad (\text{A10})$$

The phase difference $\phi(t)$ becomes a slow variable, so that it hardly changes during the period T_p . Then one can average both sides of Eq. (A10) to obtain the closed form of the evolution equation for $\phi(t)$ as

$$\frac{d\phi}{dt} = H_2(-\phi) - H_1(\phi) \equiv \Gamma(\phi), \quad (\text{A11})$$

where

$$H_i(\phi) = \int_0^1 d\theta \hat{H}_i(\theta, \phi).$$

-
- [1] J. W. Moore, *Fed. Proc.* **17**, 113 (1958).
[2] X. Cao and D. Oertel, *J. Neurophysiol.* **94**, 821 (2005).
[3] F. Berznila and R. E. Taylor, *Biophys. J.* **23**, 479 (1978).
[4] Y. Zhao and J. A. Boulant, *J. Physiol.* **564**, 245 (2005).
[5] A. L. Hodgkin and A. F. Huxley, *J. Physiol.* **117**, 500 (1952).
[6] A. L. Hodgkin, A. F. Huxley, and B. Katz, *J. Physiol.* **116**, 424 (1952).
[7] S. Kuang *et al.*, *Pramana* **70**, 183 (2008).
[8] D. J. Prior and D. S. Gega, *J. Exp. Biol.* **98**, 415 (1982).
[9] X.-J. Wang and G. Buzsáki, *J. Neurosci.* **16**, 6402 (1996).
[10] B. Ermentrout, *Neural. Comput.* **8**, 979 (1996).
[11] R. F. Galan, G. B. Ermentrout, and N. N. Urban, *Phys. Rev. Lett.* **94**, 158101 (2005).
[12] A. J. Preyer and R. J. Butera, *Phys. Rev. Lett.* **95**, 138103 (2005).
[13] T. I. Netoff, M. I. Banks, A. D. Dorval, C. D. Acker, J. S. Haas, N. Kopell, and J. A. White, *J. Neurophysiol.* **93**, 1197 (2005).
[14] D. Hansel, G. Mato, and C. Meunier, *Neural Comput.* **7**, 307 (1995).
[15] B. Gustafsson and H. Wigström, *Brain Res.* **223**, 417 (1981).
[16] T. Tateno, A. Harsch, and H. P. C. Robinson, *J. Neurophysiol.* **92**, 2283 (2004).
[17] B. N. Lundstrom, M. Famulare, L. B. Sorensen, W. J. Spain, and A. L. Fairhall, *J. Comput. Neurosci.* **27**, 277 (2009).
[18] A. Borisyuk and J. Rinzel, in *Models and Methods in Neurophysics, Proceedings Les Houches Summer School 2003, Session LXXX* (Elsevier, Dordrecht, 2005), p. 19.
[19] K. Tsumoto, H. Kitajima, T. Yoshinaga, K. Aihara, and H. Kawakami, *Neurocomputing* **69**, 293 (2006).
[20] E. M. Izhikevich, *Dynamical Systems in Neuroscience: The Geometry of Excitability and Bursting*. (MIT Press, Cambridge, MA, 2007).
[21] D. O. Carpenter, *J. Gen. Physiol.* **50**, 1469 (1967).
[22] A. S. French, *J. Comp. Physiol. A* **156**, 817 (1985).
[23] J. J. C. Rosenthal and F. Bezanilla, *Biol. Bull.* **199**, 135 (2000).
[24] M. T. Huber and H. A. Braun, *Phys. Rev. E* **73**, 041929 (2006).
[25] C. Morris and H. Lecar, *Biophys. J.* **35**, 193 (1981).
[26] H. Lecar, *Scholarpedia* **2**, 1333 (2007).

- [27] J. Keener and J. Sneyd, *Mathematical Physiology* (Springer-Verlag, New York, 1998).
- [28] H. R. Wilson, *Spikes, Decisions, and Actions: The Dynamical Foundation of Neuroscience* (Oxford University Press, New York, 1999).
- [29] W. Rall, *J. Neurophysiol.* **30**, 1138 (1967).
- [30] Y. Kuramoto, *Chemical Oscillations, Waves, and Turbulence* (Springer-Verlag, Berlin, 1984).
- [31] G. B. Ermentrout and N. Kopell, *SIAM J. Math. Anal.* **15**, 215 (1984).
- [32] F. C. Hoppensteadt and E. M. Izhikevich, *Weakly Connected Neural Networks* (Springer, New York, 1997).
- [33] B. S. Gutkin and G. B. Ermentrout, *Neural Comput.* **10**, 1047 (1998).
- [34] C. I. Buia and P. H. Tiesinga, *J. Neurophysiol.* **99**, 2158 (2008).
- [35] N. Ishiko and W. R. Loewenstein, *J. Gen. Physiol.* **45**, 105 (1961).
- [36] M. J. Beilby and H. G. J. Coster, *Aust. J. Plant Physiol.* **3**, 275 (1976).
- [37] S. Marella and G. B. Ermentrout, *Phys. Rev. E* **77**, 041918 (2008).
- [38] Y. Tsubo, M. Takada, A. D. Reyes, and T. Fukai, *Euro. J. Neurosci.* **25**, 3429 (2007).
- [39] Y. Tsubo, J.-N. Teramae, and T. Fukai, *Phys. Rev. Lett.* **99**, 228101 (2007).
- [40] J. B. Peloquin, C. J. Doering, R. Rehak, and J. E. McRory, *Neuroscience* **151**, 1066 (2008).
- [41] K. Matsumoto, T. Ueda, and Y. Kobatake, *J. Theor. Biol.* **131**, 175 (1988).
- [42] T. Nakagaki, H. Yamada, and T. Ueda, *Biophys. Chem.* **84**, 195 (2000).
- [43] A. Mehrotra and A. Sangiovanni-Vincentelli, *Noise Analysis of Radio Frequency Circuits* (Kluwer, Dordrecht, 2004).
- [44] Y. D. Sato, Ph.D. thesis, Tokyo Institute of Technology, 2005 (unpublished).